International Journal of Thermal Sciences 48 (2009) 1265–1272

Contents lists available at ScienceDirect

International Journal of Thermal Sciences

www.elsevier.com/locate/ijts

Mixed convection in a double lid-driven cubic cavity

Nasreddine Ouertatani [a,*], Nader Ben Cheikh [a], Brahim Ben Beya [a], Taieb Lili [a], Antonio Campo [b]

[a] Département de Physique, Faculté des Sciences de Tunis, Campus Universitaire, 2092 El-Manar II, Tunisia
[b] Department of Mechanical Engineering, The University of Texas at San Antonio, San Antonio, TX 78249, USA

ARTICLE INFO

Article history:
Received 22 July 2008
Received in revised form 8 November 2008
Accepted 26 November 2008
Available online 20 December 2008

Keywords:
Three-dimensional analysis
Double lid-driven cubic cavity
Mixed convection
Numerical simulation
Multigrid method

ABSTRACT

To study the intricate three-dimensional flow structures and the companion heat transfer rates in double lid-driven cubic cavity heated from the top and cooled from below, a numerical methodology based on the finite volume method and a full multigrid acceleration is utilized in this paper. The four remaining walls forming the cubic cavity are adiabatic. The working fluid is air so that the Prandtl number equates to 0.71. Numerical solutions are generated for representative combinations of the controlling Reynolds number inside $100 \leqslant Re \leqslant 1000$ and the Richardson numbers inside $0.001 \leqslant Ri \leqslant 10$. Typical sets of streamlines and isotherms are presented to analyze the tortuous circulatory flow patterns set up by the competition between the forced flow created by the double driven walls and the buoyancy force of the fluid. For extreme combinations of high *Ri* and low *Re*, the heat transfer is essentially dominated by conduction. On the other hand, for extreme combinations of small *Ri* and high *Re*, the heat transfer becomes convective dominating. Numerical values of the overall Nusselt number in harmony with the *Re*- and *Ri*-intervals are presented and they are compared afterward against the standard case of a single lid driven cavity. It is discovered that a remarkable heat transfer improvement of up to 76% can be reached for the particular combination of $Re = 400$ and $Ri = 1$.

1. Introduction

The problem on laminar mixed convection with lid driven flows has multiple applications in the field of thermal engineering. Such problems are of great interest, for example in electronic device cooling, high-performance building insulation, multi shield structures used for nuclear reactors, food processing, glass production, solar power collectors, furnace, drying technologies, etc. Numerous studies on lid-driven cavity flow and heat transfer involving different cavity configurations, various fluids and imposed temperature gradients have been continually published in the literature.

The numerical simulations of Moallemi and Jang [1] focused on two-dimensional laminar flow induced by Reynolds number ($100 \leqslant Re \leqslant 2200$), and small-to-moderate Prandtl number ($0.01 \leqslant Pr \leqslant 50$) on the flow and heat transfer features in a cavity for different levels of the Richardson numbers. These authors found that the influence of buoyancy on the flow and heat transfer to be more pronounced for higher values of *Pr*, if *Re* and *Gr* are kept constant. The natural convection contribution always assists the forced convection magnitude, and the extent of the net result responds to a function of *Pr* and *Ri*.

Sharif [2] performed a numerical investigation with supplementary flow visualization of laminar mixed convective heat transfer in two-dimensional shallow rectangular driven cavities of aspect ratio 10. The top moving plate of the cavity is set at a higher temperature than the bottom stationary plate. Computations are reported for Rayleigh numbers ranging from 10^5 to 10^7 while keeping the Reynolds number fixed at 408.21, thus encompassing the wide spectrum of dominating forced convection, mixed convection, and dominating natural convection flow regimes. The fluid Prandtl number is taken as 6, representative of water. The effects of inclination of such a cavity on the flow and thermal fields are also investigated for inclination angles ranging from 0° to 30°. The author observed that the local Nusselt number at the heated moving plate starts with a high value and decreases rapidly to a small value towards the right side. The local Nusselt number at the cold plate reveals certain oscillatory behavior near the right side due to the presence of a separation bubble at the cold surface in that location. It was concluded in [2] that the average or overall Nusselt number increases mildly with cavity inclination for the dominant forced convection case dictated by ($Ri = 0.1$). In contrast, it increases much more rapidly with inclination for the other dominant natural convection case dictated by ($Ri = 10$).

Prasad et al. [3] numerically studied mixed convection inside a rectangular cavity where the two vertical walls are maintained at cold temperature ($T = 0$). In one case, the top-moving wall is maintained at hot temperature ($T = 1$) and the bottom is at a cold temperature ($T = 0$) and in the other case, the top is at a cold temperature ($T = 0$) and the bottom is at a hot temperature ($T = 1$). They concluded that when the negative *Gr* is increased, a strong

* Corresponding author.
E-mail address: nasreddine_ouertatani@yahoo.fr (N. Ouertatani).

1290-0729/$ – see front matter
doi:10.1016/j.ijthermalsci.2008.11.020

Nomenclature

H	side of cubic cavity
g	gravitational acceleration
Gr	Grashof number, $g\beta(T_{HOT} - T_{COLD})H^3/\nu^2$
m	iteration level
n	normal direction
Nu	mean Nusselt number
Nu_{loc}	local Nusselt number
p	non-dimensional pressure
p_0	pressure scale, ρu_0^2
Pr	Prandtl number, ν/α
Re	Reynolds number, $u_0 H/\nu$
Ri	Richardson number, Gr/Re^2
t	non-dimensional time
t_0	time scale, H/u_0
T	temperature
T_{COLD}	temperature of cold wall
T_{HOT}	temperature of hot wall
u_0	velocity scale
u, v, w	non-dimensional velocities
x, y, z	non-dimensional Cartesian coordinates

Greek symbols

α	thermal diffusivity of the fluid
β	coefficient of thermal expansion of the fluid
ν	kinematic viscosity
θ	non-dimensional temperature, $(T - T_C)/(T_H - T_C)$
ρ	density

convection is manifested for aspect ratios equal to 0.5 and 1.0. Even more, a Hopf bifurcation occurs at $Gr = -10^5$ for the aspect ratio 2. In this situation, the flow does not remain steady any longer and becomes transient. Mohammad and Viskanta [4] numerically examined two and three-dimensional laminar flow and heat transfer in a Rayleigh–Bénard container. They established that the lid motion annihilates all forms of convective cells due to heating from below for finite size cavities. Aydin et al. [5] conducted a numerical investigation to analyze the transport mechanism of mixed convection in a shear and buoyancy-driven cavity having a locally heated lower wall and moving cooled sidewalls. In addition, other numerical studies such as Han and Kuehn [6] and Oztop and Dagtekin [7] were carried out on this topic. Iwatsu et al. [8] performed a numerical investigation on the effect of external excitation on the flow structure in a square cavity. The results of the two publications have shown a similar flow structure to steady driven-cavity flows when utilizing small frequency values. Such a similarity, however, vanished when large frequency values were implemented. A subsequent work by Iwatsu et al. [9] carried out a numerical study of the viscous flow in a heated driven-cavity under thermal stratification, where the oscillating lid was maintained at a temperature higher than the lower wall. Their collection of results had revealed significant augmentation in heat transfer rate at particular lid frequency values, which convincingly indicates the existence of the resonance phenomena.

A detailed literature survey reveals that the majority of existing numerical investigations are restricted to two-dimensional configurations. In this vein, 2D models are deficient because they do not always capture the intricacies inherent to the flow behavior realistically. Owing to these shortcomings, 3D models have to be undertaken to guarantee accuracy. A limited number of articles fall into this general category and have been reported in the literature. Among others, Iwatsu [10] numerically studied three-dimensional mixed convective flows in a cubical container with a steady vertical temperature stratification. He observed that the three-dimensional effects are intensified as Re increases. Mohammad and Viskanta [11] conducted three-dimensional numerical simulation of mixed convection in a shallow driven cavity heated from the top moving wall and cooled from below. The cavity was filled with a stably stratified fluid encompassing a relative large range of Rayleigh number and Richardson number. In a sequence of papers, Freitas et al. [12] and Freitas and Street [13] carried out a numerical study of the viscous flow in a rectangular cavity of depth-to-spanwise aspect ratio 3 at $Re = 3200$. They discovered the existence of meridional vortices and considerable flow unsteadiness.

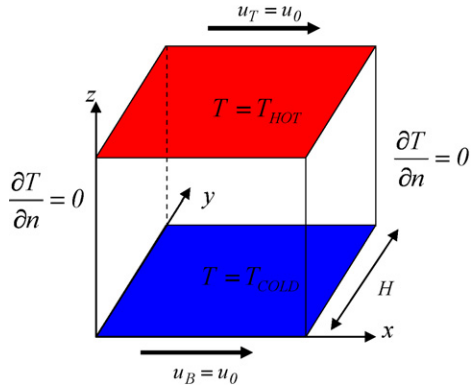

Fig. 1. Physical system and Cartesian coordinates.

In view of the foregoing statements, it seems that the problem of three-dimensional laminar mixed convection heat transfer in a cubic cavity heated from the top hot moving lid and cooled from the bottom cold moving lid has not been addressed yet. In this paper, we undertake this task varying the Reynolds number in the Re-interval $(100 \leqslant Re \leqslant 1000)$ and the Richardson number in the Ri-interval $(0.001 \leqslant Ri \leqslant 10)$ for air $(Pr = 0.71)$ as the working fluid. The transport processes will be investigated with the finite volume method and the discussion will revolve around the precise determination of temporal velocity and temperature fields. In addition, the temporal variation of the average Nusselt number will be documented for all cases studied.

The paper is organized as follows. In the second section the physical system is formulated. The numerical methodology is briefly described in the third section and subsequently validated. The computed results are presented and discussed in the fourth section. In the final section, the most important findings of this study are summarized.

2. Physical system

The physical system under study is sketched in Fig. 1. It basically consists of a double-lid cubic cavity with side H filled with air $(Pr = 0.71)$. The applicable flow and temperature boundary conditions are described next. The bottom and top lids impart a steady sliding motion in the same direction sharing the uniform velocity $u_B = u_T = u_0$, while the other four walls are stationary. The top and bottom moving lids are maintained at uniform temperatures, the top lid has a temperature T_{HOT}, the bottom lid has a temperature T_{COLD} wherein $T_{HOT} > T_{COLD}$. In addition, the remaining walls are considered adiabatic.

3. Numerical methodology and algorithm validation

The governing equations for unsteady, incompressible laminar flow consist of the continuity equation, three Navier–Stokes equations accounting for the Boussinesq approximation and the energy equation. The non-dimensional equations are collectively written in tensor notation as follows:

Continuity equation:

$$\frac{\partial u_i}{\partial x_i} = 0, \tag{1}$$

Three momentum equations:

$$\frac{\partial u_i}{\partial t} + \frac{\partial (u_i u_j)}{\partial x_j} = -\frac{\partial p}{\partial x_i} + \frac{1}{Re}\left(\frac{\partial^2 u_i}{\partial x_i \partial x_i}\right) + Ri\,\theta\,\delta_{i3}, \tag{2}$$

Energy equation:

$$\frac{\partial \theta}{\partial t} + \frac{\partial (u_i \theta)}{\partial x_i} = \frac{1}{Ra\,Pr}\left(\frac{\partial^2 \theta}{\partial x_i \partial x_i}\right) \tag{3}$$

where $u_i = (u; v; w)$ are the velocity components, p is the kinematic pressure, and θ is the temperature, ρ is the mass density, and g is the gravitational acceleration. In Eq. (2), the symbol δ_{ij} stands for the Krönecker delta. The chosen scales in Eqs. (1)–(3) are the side H, the velocity $u_0 = \sqrt{g\beta H \Delta T}$, the time $t_0 = H/u_0$ and the pressure $p_0 = \rho u_0^2$. Further, the non-dimensional temperature is defined by $\theta = (T - T_R)/(T_{HOT} - T_{COLD})$, where the reference temperature $T_R = (T_{HOT} + T_{COLD})/2$ and the temperature scale is the lid-to-lid temperature difference $(T_{HOT} - T_{COLD})$.

In light of the foregoing, the forced-natural convection problem is characterized by three non-dimensional parameters: (1) the Reynolds number $Re = \frac{U_0 H}{\nu}$ where U_o is the impressed lid velocity; (2) the Prandtl number $Pr = \nu/\alpha$, where ν is the kinematic viscosity, α the thermal diffusivity of the fluid; (3) the Grashof number $Gr = \beta g \Delta T H^3/\nu^2$ in which β is the coefficient of thermal expansion of the fluid, g the gravity and $\Delta T = T_{HOT} - T_{COLD}$ the temperature difference between the hot and cold horizontal walls. Alternatively, Gr and Re are adequately blended in the mixed-convection parameter called the Richardson number $Ri = Gr/Re^2$.

The unsteady Navier–Stokes and energy equations are discretized by a second-order time stepping finite difference procedure. The procedure adopted here deserves a detailed explanation. First, the non-linear terms in Eqs. (2) are treated explicitly with a second-order Adams–Bashforth scheme. Second, the convective terms in Eq. (3) are treated semi-implicitly. Third, the diffusion terms in Eqs. (2) and (3) are treated implicitly. In order to avoid the difficulty that the strong velocity-pressure coupling brings forward, we selected a projection method described in Peyret and Taylor [14] and Achdou and Guermond [15].

A finite-volume method is implemented to discretize the Navier–Stokes and energy equations (Patankar [16], F. Moukhalled and M. Darwish [17], Kobayachi and Pereira and Pereira [18]). The advective terms in Eqs. (2) are discretized using a QUICK third-order scheme whereas a second-order central differencing (Hayase, Humphrey and Greif [19]) is applied in Eq. (3). The discretized momentum and energy equations are solved employing the red and black successive over relaxation method (RBSOR) in Press et al. [20], while the Poisson pressure correction equation is solved utilizing a full multi-grid method (Hortmann, Peric and Scheuerer [21], M.S. Mesquita and M.J.S. de Lemos [22], E. Nobile [23]). If specific details about the computational methodology are needed, the reader is directed to Ben Cheikh et al. [24]. Finally, the convergence of the numerical 3D velocity field and the 3D temperature field is established at each time step when all residuals are forced to stay below 10^{-6}. To secure steady state conditions the following criterion has to be satisfied:

$$\sum_{i,j,k} \left| \Phi^{m+1}_{i,j,k} - \Phi^{m}_{i,j,k} \right| \leqslant 10^{-5} \tag{4}$$

where the generic variable Φ represents the set of four variables u, v, w or θ. In the above inequality, the superscript m indicates the iteration number and the subscript sequence (i, j, k) represents the space coordinates x, y, z.

For enhanced accuracy, the present numerical model was checked against the published numerical solution of [10], which is based on a finite volume scheme for three-dimensional driven-cavity flows, but with an imposed vertical temperature gradient. The outcomes of the one-to-one comparisons are documented in Table 1 for the average Nusselt number predictions. It is observed here that the present numerical computations match very closely those of [10].

Table 1
Comparison of the computed average Nusselt number at the top wall.

Re	*Ri* = 0.001			*Ri* = 1.0			*Ri* = 10.0		
	Ref. [16]	Pres. work	Diff. (%)	Ref. [16]	Pres. work	Diff. (%)	Ref. [16]	Pres. work	Diff. (%)
100	1.82	1.836	0.9	1.33	1.348	1.2	1.08	1.092	1.1
400	3.99	3.964	−0.7	1.50	1.528	1.9	1.17	1.130	−3.4
1000	7.03	7.284	3.6	1.80	1.856	3.1	1.37	1.143	−16.6

4. Results and discussion

The computed mixed convection flow and temperature fields in the two-sided lid-driven cubic cavity are examined in this section. The numerical results are presented in terms of streamlines, isotherms culminating with the local Nusselt numbers. The Reynolds number Re is varied two orders of magnitude between 100 and 1000. In addition, the Richardson number Ri is varied four orders of magnitude between 0.001 and 10. The Prandtl number is set at $Pr = 0.71$. We ran computations for nine different pairs of Ri and Re; that is: $(Ri, Re) = (10, 100)$, $(10, 400)$, $(10, 1000)$, $(1, 100)$, $(1, 400)$, $(1, 1000)$, $(0.001, 100)$, $(0.001, 400)$ and $(0.001, 1000)$. In harmony with this, the implications of varying Ri and Re will be adequately highlighted.

A series of trial calculation were conducted with two different variable grid distributions, i.e., $64 \times 64 \times 64$ and $80 \times 80 \times 80$. For the moderate case dealing with $Re = 400$ and $Ri = 1.0$, minor differences of less than 0.4% were detected between the flow and temperature results produced by the grid $64 \times 64 \times 64$ and those by the grid $80 \times 80 \times 80$. Consequently, to optimize the grid distribution appropriately, the grid $64 \times 64 \times 64$ was deemed adequate to perform all numerical computations. For completeness, the two grids were built using a tangent hyperbolic formulation. The smallest space intervals chosen in the three coordinate directions are $\Delta x_{min} = \Delta y_{min} = \Delta z_{min} = 5 \times 10^{-3}$, and are localized near the moving and stationary walls to capture the growth of the flow and thermal boundary layers adjacent to them. Tiny time steps were confined to the interval $5 \times 10^{-3} \leqslant \Delta t \leqslant 10^{-2}$ depending on the magnitudes of Richardson and Reynolds numbers.

4.1. Flow structure

The trajectory of particles for the different envisaged cases is shown in Fig. 2. We note that for the lowest Reynolds number employed ($Re = 100$), the influence of the Richardson number upon the overall structure of the flow is practically insignificant. Besides, it is noticeable in Figs. 2a, 2b and 2c the presence of two counter-rotating cells localized in the proximity of the two moving lids;

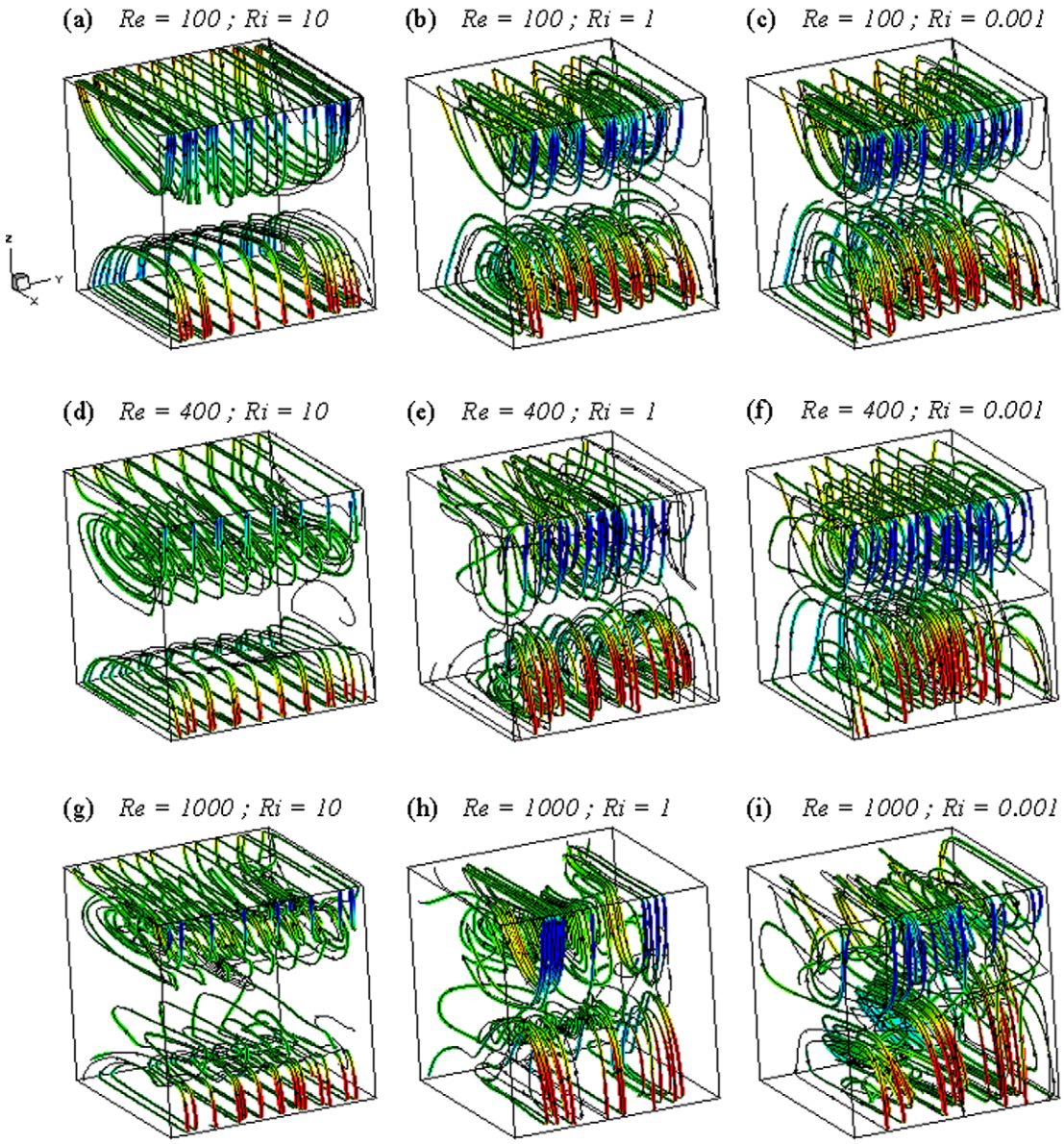

Fig. 2. The trajectory of particles for different combinations of *Re* and *Ri*.

their intensity is slightly modified when *Ri* decreased. The mid-plane streamlines distributions for designated values of *Re* and *Ri* are displayed in Fig. 3. Despite the variability in *Re* and *Ri*, a very definite symmetry of the fluid motion is prevalent. When *Re* and *Ri* are set at 100 and 10, respectively, the flow patterns are characterized by two primary recirculating clockwise vortex that are similar in size. This behavior is primarily due to the lid movement that occupy the region near the sliding top and bottom lids. In addition, two minor secondary recirculating vortices due to buoyancy were observed between the two main cells. With decrements in *Ri*, the secondary cells becomes feeble and amalgamate with the primary cells to provide only two extensive vortex. Interestingly, it is also noticed that the direction of the lid velocities cause the centres of the vortex to move from the left side to the right side as confirmed in Figs. 3b and 3c. Moreover, this physical model is a constituent for a vertical stratification to be conserved in the integrated cubic cavity. Fundamentally speaking, this signifies that the cavity lies in a quasi-conduction domain, i.e., most of the heat transfer seems to be due to conduction excluding the heat transfer in close proximity to the top and bottom lids.

When *Ri* decreases to 0.001, the forced convection regime invigorates and eclipses its conduction counterpart. Furthermore the all-embracing flow patterns persist fairly unchanged. This in fact is ascribed to the inherent enhancement in the involvement of convection heat mechanism, which causes abrupt temperature gradients in the vertical direction in the vicinity of the top lid. It seems that the buoyancy forces are submerged by the mechanical effect generated by the two moving lids. For moderate *Re*, i.e., $Re = 400$, the Richardson number *Ri* has a marked effect on the overall flow structure. As shown in Fig. 3d, the two secondary cells occupying much of the cavity basically retain the same symmetry. When *Ri* diminishes to 1 and thereafter to 0.01, as indicated in Figs. 3e and 3f, the two vortices localized near the two moving lids are found to amalgamate with the vortices of the core filling much of the cubic cavity. It is constantly perceived that the positive lid velocity causes the vortex center to move from left to right.

For $Re = 1000$ and $Ri = 10$, the flow patterns are characterized by six cells that occupy the entire cubic cavity as reflected in Fig. 3g. With the reduction in *Ri*, i.e., $Ri = 1$ the secondary cells are gradually weakened, namely four cells appearing in Fig. 3h and finally two cells appearing in Fig. 3i for $Ri = 0.001$. It is worth not-

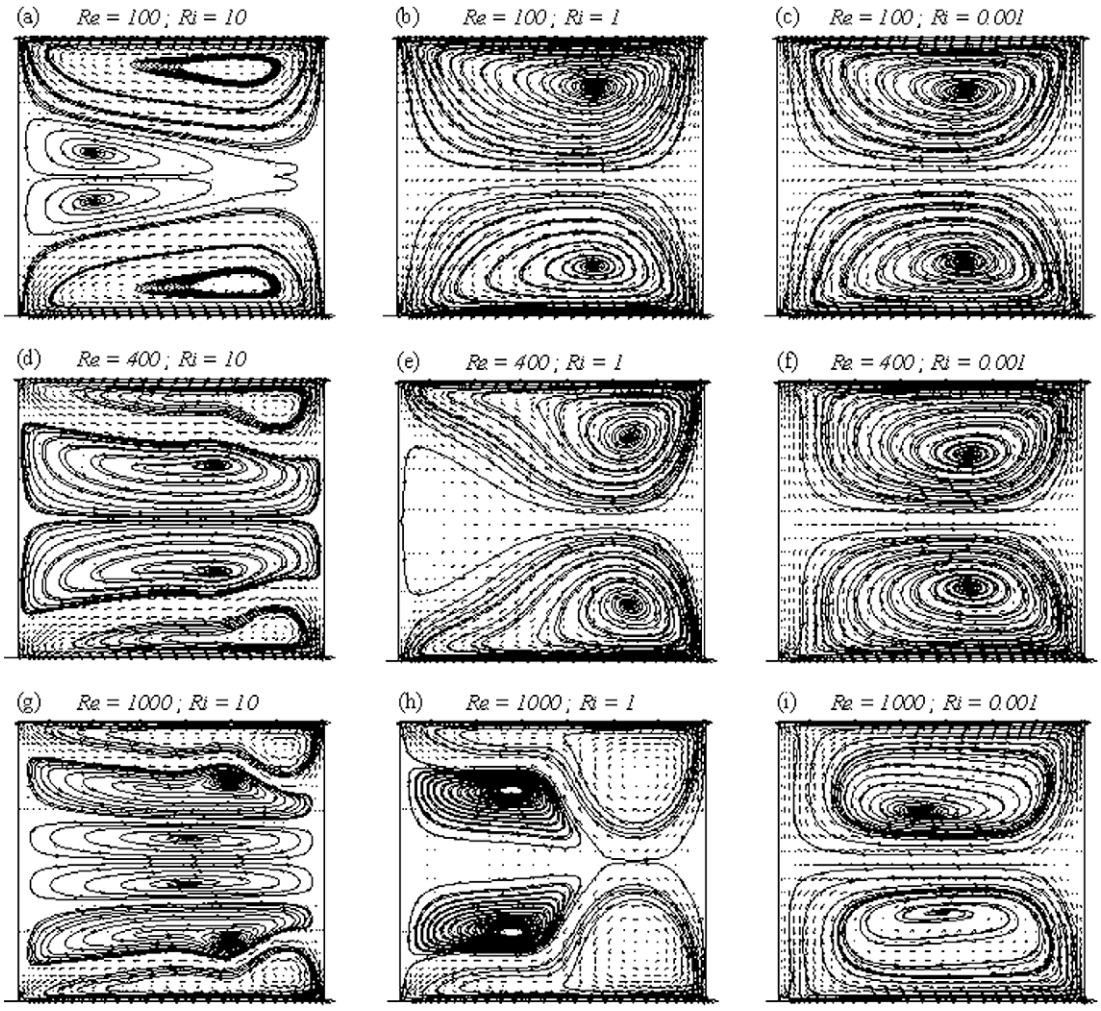

Fig. 3. Velocity vectors at the x–z mid-planes for different combinations of Re and Ri.

ing that progressively with the decrease in Ri and the increase in Re, the convection net effect in heat transfer experiences some degree of augmentation. The results also point out to the fact that when Ri is small, say of the order of $Ri \leqslant 1$, the flow is basically responsive to the lids-movement; in other words, convection due to the buoyancy effect is absent. Accordingly, it may be inferred that the convection heat transfer has become the principal energy carrier in these cases. When Re is convincingly small ($Re = 100$) and Ri is large, the prevalent influence of buoyancy is palpable.

At this juncture, it is important to mention that, for the two last cases ($Re = 1000$ united to $Ri = 1$) and ($Re = 1000$ united to $Ri = 0.001$), the particle trajectories become more tortuous as corroborated in the tandem of Figs. 2h and 2i. The two figures clearly display the impact that Re and Ri exert on the basic character of the flow and the undeniable three-dimensional comportment. Furthermore, the asymmetry observed in Fig. 2i for $Re = 1000$ coupled with $Ri = 0.001$ is certainly due to the fact that the flow becomes intrinsically periodic. To save journal space, the instability study is not included in the present paper which is solely devoted to three-dimensional calculations.

4.2. Heat transfer characteristics

Fig. 4 illustrates the influence of varying Re and Ri on the isotherms for the nine cases studied. In Figs. 4a, 4d and 4g, the results convincingly indicate that when Ri is set at 10, the isotherms exhibit similar trends for different Re. Consequently, the collective behavior attests the impact that Re exerts on heat transfer is insignificant. Accordingly, since the buoyancy is high ($Ri = 10$), the temperature contours embody a thermally stratified situation. In other words, the flow is principally dominated by buoyancy and the heat transfer is controlled mainly by conduction, implying that forced convection due to the lids-movement is almost absent. In contrast, as Ri decreases to $Ri = 1$ and Re is feeble i.e., $Re = 100$ Fig. 4b eyewitnesses that the buoyancy effects remain dominant.

The isotherm patterns at higher Re are described in Figs. 4e, 4f and 4h sequentially. As Re is gradually enlarged from 400 up to 1000, whereas Ri remains very small ($Ri = 1$ and $Ri = 0.001$), the three-dimensional characteristics of the isotherm patterns are manifested in Figs. 4e, 4f and 4h. In all fairness, it is clearly discernible that the mechanically driven forced convection dominates the buoyancy-driven convection. In addition, same observations deserve further clarification when $Ri = 0.001$ and $Re = 1000$. In here, an asymmetry of the thermal field appears as can be confirmed in Fig. 4i. This particular figure highlights the presence of flow instability which was evoked in the preceding paragraph.

In order to assess the local heat transfer distribution along the hot moving lid, the local Nusselt number is defined by:

$$Nu_{\mathrm{loc}} = -\left.\frac{\partial\theta}{\partial z}\right|_{z=1}, \tag{5}$$

and plotted in Fig. 5 for all the cases studied. The joint effect of varying Re and Ri upon the heat transfer process is undoubtedly noticeable in these plots. It is clearly observed that

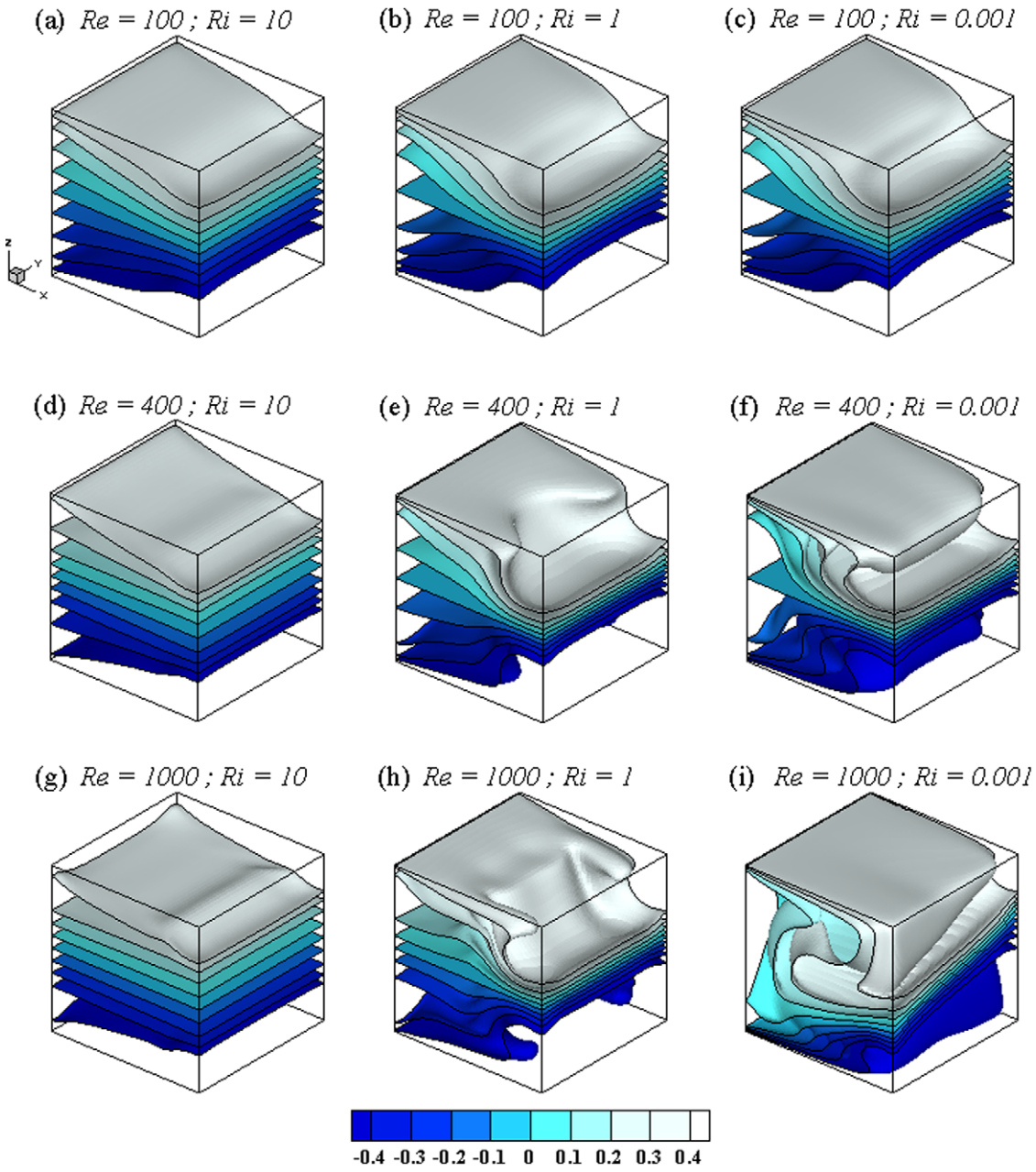

Fig. 4. The isotherm plots.

the local Nusselt number patterns are in good agreement with the isotherm plots previously commented. For instance, for larger $Ri = 1$ and 10 connected to Figs. 5a and 5b, the local Nusselt numbers are significantly small and the Nu_{loc} distributions are literally two-dimensional. This simply translates into a conduction dominant scenario. With increments in *Re* and decrements in *Ri*, the end product consists in elevations in Nu_{loc}. Hence, the convection mode in heat transfer is predominant as witnessed in Figs. 5e, 5f, 5h and 5i. Furthermore, maximum heat transfer is attained at the upstream part of the top moving lid and minimum at the downstream part.

When *Re* is large, the local Nusselt numbers are very large at the corners of the upstream top moving lid. This intensification indicates that the fluid motions are invigorated in the upper region of the cubic cavity. Consequently, heat transfer is controlled mainly by the convection mode.

Table 2 lists the average Nusselt number *Nu* at the top moving lid for the computations obtained. It is noteworthy that *Nu* attains very large values of the order of $Nu > 2$ whenever *Re* and *Ri*. This tendency is attributed to an extra contribution of the convection heat transfer mechanism, which causes steep temperature gradients in the vertical direction in close proximity to the top lid. It seems that, the influence of buoyancy forces are overwhelmed by the viscous forces induced by the two moving lids.

From the comparison between the items included in Tables 1 and 2, it appears that the average heat transfer for the case of the cubic cavity with two moving lids is superior to that corresponding to the cubic cavity with one moving lid. In sum, it is important to culminate the discussion highlighting the qualitative differences between the two cases amounting to 10.2%, 13.1%, 13.6%, 26.5%, 76%, 65.8%, 0.1%, 4.9% et 9.6% for the pairs $(Ri; Re) = (10; 100)$, $(10; 400)$, $(10; 1000)$, $(1; 100)$, $(1; 400)$, $(1; 1000)$, $(0.001; 100)$, $(0.001; 400)$ and $(0.001; 1000)$, respectively, as reported in Fig. 6. It is worth adding that the maximum differences happen for $Ri = 1$ in conjunction with $100 \leqslant Re \leqslant 1000$.

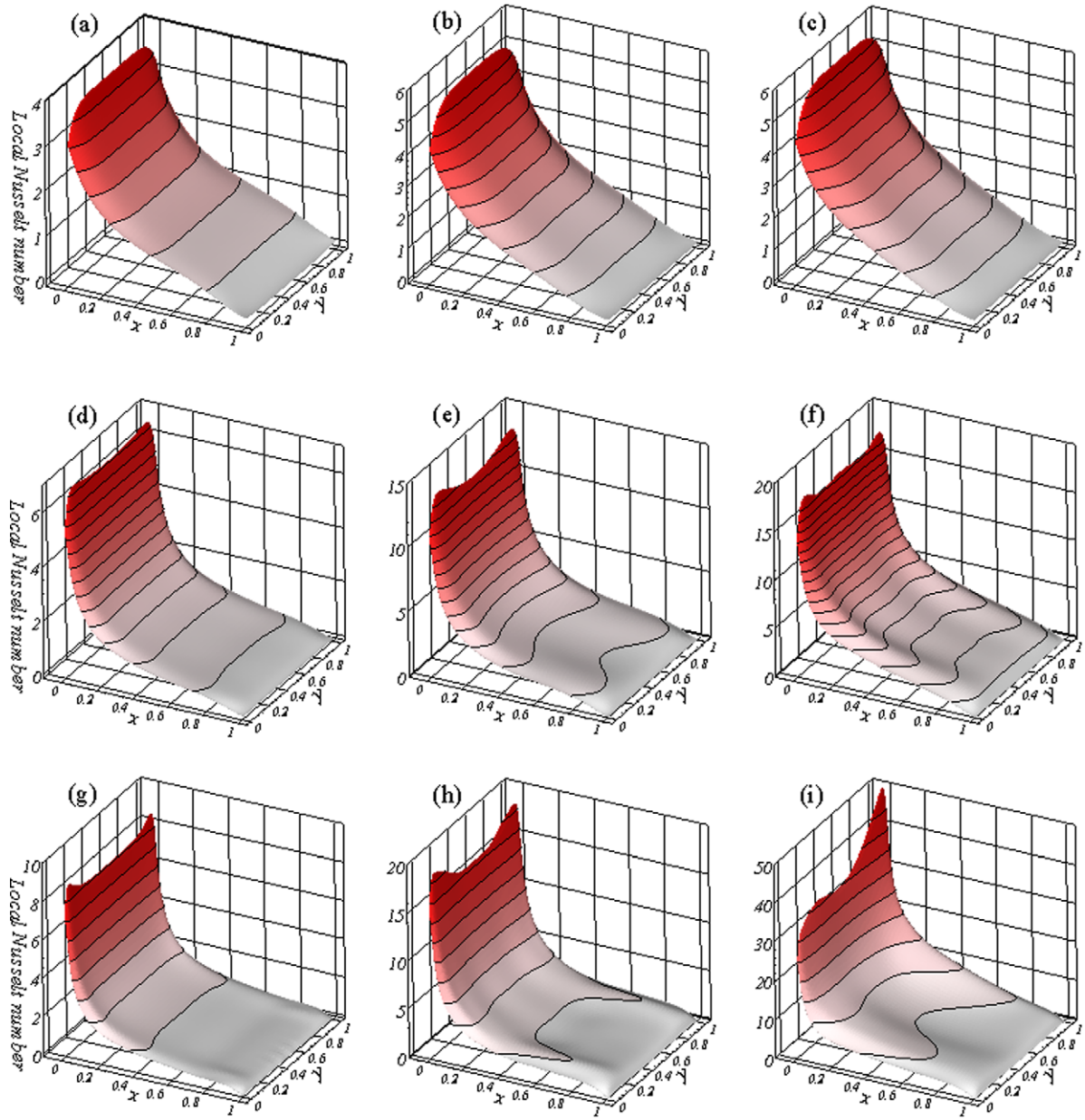

Fig. 5. The contour values of local Nusselt number related to various combinations: (a) $Re = 100$ and $Ri = 10$, (b) $Re = 100$ and $Ri = 1$, (c) $Re = 100$ and $Ri = 0.001$, (d) $Re = 400$ and $Ri = 10$, (e) $Re = 400$ and $Ri = 1$, (f) $Re = 400$ and $Ri = 0.001$, (g) $Re = 1000$ and $Ri = 10$, (h) $Re = 1000$ and $Ri = 1$, (i) $Re = 1000$ and $Ri = 0.001$.

Table 2
The average Nusselt number *Nu* at the top moving lid for the computations obtained.

Re	$Ri = 0.001$	$Ri = 1.0$	$Ri = 10.0$
100	1.838	1.705	1.204
400	4.160	2.688	1.278
1000	7.983	3.079	1.299

5. Conclusion

The current investigation addressed three-dimensional laminar mixed convection in a double lid-driven cubic cavity filled with air ($Pr = 0.71$) for suitable combinations of three different Reynolds numbers and three different Richardson numbers. The effects of varying both Reynolds and Richardson numbers on the resulting convection are investigated. Interesting behaviors of the flow and thermal fields with varying Reynolds and Richardson numbers are observed. When large *Ri* is united with low *Re*, two primary vortex

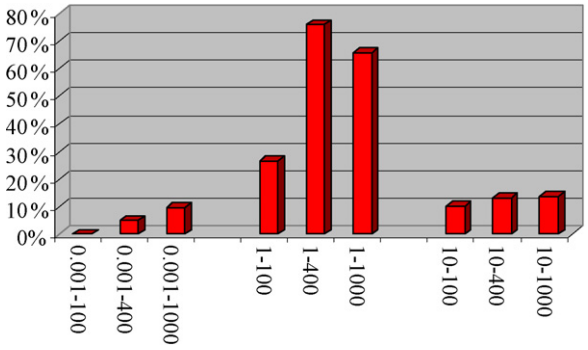

Fig. 6. Percentage difference as a function of both *Ri* and *Re*.

are observed circumscribed in the proximity of the two moving lids and their intensity is slightly modified when *Ri* decreased. In addition, two minor secondary recirculating vortices were observed between the two main cells. Furthermore, the isotherm

surfaces preserve a fair degree of two-dimensionality. In this case, the buoyancy influence is dominant. When *Ri* is small and *Re* is large, three-dimensionalities of the isotherm patterns are manifested. The flow is basically carried by the lids movement. In this case the mechanically driven convection is dominant. The heat transfer characteristics inside the cubic cavity are improved significantly for low values of *Ri* due to the dominant effect of the mechanical effect provoked by the moving lids. When large *Re* is paired with very low *Ri* the flow becomes periodic and the symmetry of the flow is broken. The effects of both *Re* and *Ri* are also apparent in the plots of the local Nusselt number. For high *Ri*, the conduction mode dominates the picture. However, when *Ri* is small, and especially when *Re* is large, the heat transfer rate increases due to the dominant forced convection. Numerical results also demonstrate that the average heat transfer for the case of the cubic cavity with two moving lids is superior to that in the case of the cubic cavity with only one moving lid. Indeed, a remarkable improvement of up to 76% can be reached for the specific combination $(Ri, Re) = (1, 400)$.

References

[1] M.K. Moallemi, K.S. Jang, Prandtl number effects on laminar mixed convection heat transfer in a lid-driven cavity, Int. J. Heat Mass Transfer 35 (1992) 1881–1892.

[2] M.A.R. Sharif, Laminar mixed convection in shallow inclined driven cavities with hot moving lid on top and cooled from bottom, Applied Thermal Engineering 27 (2007) 1036–1042.

[3] Y.S. Prasad, M.K. Das, Hopf bifurcation in mixed flow inside a rectangular cavity, Int. J. Heat Mass Transfer 50 (2007) 3583–3598.

[4] A.A. Mohammad, R. Viskanta, Laminar flow and heat transfer in Rayleigh–Benard convection with shear, Phys. Fluids A 4 (1992) 2131–2140.

[5] O. Aydin, W.-J. Yang, Mixed convection in cavities with a locally heated lower wall and moving sidewalls, Numer. Heat Transfer, Part A: Applications 37 (2000) 695–710.

[6] H. Han, T.H. Kuehn, A numerical simulation of double diffusive convection in a vertical rectangular enclosure, ASME HTD 107 (1989) 149–154.

[7] H.F. Oztop, I. Dagtekin, Mixed convection in two sided lid driven differentially heated square cavity, Int. J. Heat Mass Transfer 47 (2004) 1761–1769.

[8] R. Iwatsu, J.M. Hyun, K. Kuwahara, Numerical simulation of flows driven by a torsionally oscillating lid in a square cavity, J. Fluids Engineering. 114 (1992) 143–151.

[9] R. Iwatsu, J.M. Hyun, K. Kuwahara, Convection in a differentially-heated square cavity with a torsionally-oscillating lid, Int. J. Heat Mass Transfer 35 (1992) 1069–1076.

[10] R. Iwatsu, J.M. Hyun, Three-dimensional driven-cavity flows with a vertical temperature gradient, Int. J. Heat Mass Transfer 38 (1995) 3319–3328.

[11] A.A. Mohammad, R. Viskanta, Flow and heat transfer in a lid-driven cavity filled with a stably stratified fluid, Appl. Math. Modelling 19 (1995) 465–472.

[12] C.J. Freitas, R.L. Street, A.N. Findikakis, J.R. Koseff, Numerical simulation of three-dimensional flow in a cavity, Int. J. Numer. Meth. Fluids 5 (1985) 561–575.

[13] C.J. Freitas, R.L. Street, Non-linear transport phenomena in a complex recirculating flow: a numerical investigation, Int. J. Numer. Meth. Fluids 8 (1988) 769–802.

[14] R. Peyret, T.D. Taylor, Methods for Fluid Flow, Springer-Verlag, Berlin, Germany, 1983.

[15] Y. Achdou, J.L. Guermond, Convergence analysis of a finite element projection/Lagrange–Galerkin method for the incompressible Navier–Stokes equations, SIAM J. Numer. Anal. 37 (2000) 799–826.

[16] S.V. Patankar, A calculation procedure for two-dimensional elliptic situations, Numer. Heat Transfer 34 (1981) 409–425.

[17] F. Moukhalled, M. Darwish, A unified formulation of the segregated class of algorithm for fluid flow at all speeds, Numer. Heat Transfer, Part B: Fundamentals 37 (2000) 103–139.

[18] M.H. Kobayachi, J.M.C. Pereira, J.C.F. Pereira, A conservative finite-volume second-order-accurate projection method on hybrid unstructured grids, J. Comput. Phys. 150 (1999) 40–75.

[19] T. Hayase, J.A.C. Humphrey, R. Greif, A consistently formulated QUICK scheme for fast and stable convergence using finite-volume iterative calculation procedures, J. Comput. Phys. 98 (1992) 108–118.

[20] W.H. Press, et al., second edition, Numerical Recipes in Fortran 77: The Art of Scientific Computing, vol. 1, Cambridge Press, London, UK, 1997.

[21] M. Hortmann, M. Peric, G. Scheuerer, Finite volume multigrid prediction of laminar natural convection: benchmark solutions, Int. J. Numer. Meth. Fluids 11 (1990) 189–207.

[22] M.S. Mesquita, M.J.S. de Lemos, Optimal multigrid solutions of dimensional convection–conduction problems, Appl. Math. Comput. 152 (2004) 725–742.

[23] E. Nobile, Simulation of time-dependent flow in cavities with the correction multigrid method, Part I: Mathematical formulation, Numer. Heat Transfer, Part B: Fundamentals 30 (1996) 341–350.

[24] N.B. Cheikh, B.B. Beya, T. Lili, Natural convection flow in a tall enclosure using a multigrid method, Compte Rendu Mécanique 335 (2007) 113–118.